Sliding Mode and Super-Twisting Sliding Mode Control Structures for Vertical Three-Tank Systems

Claudia-Adina BOJAN-DRAGOS[1], Radu-Emil PRECUP[1,2]*, Emil M. PETRIU[3], Robert-Alexander TIBRE[1], Tabita HAN[1]

[1] Department of Automation and Applied Informatics, Politehnica University of Timisoara, 2 V. Parvan Avenue, 300223 Timisoara, Romania
claudia.dragos@upt.ro, radu.precup@aut.upt.ro (**Corresponding author*), robert.tibre@student.upt.ro, tabita.han@student.upt.ro

[2] Center for Fundamental and Advanced Technical Research, Romanian Academy - Timisoara Branch, 24 Mihai Viteazu Avenue, 300223 Timisoara, Romania
radu.precup@upt.ro

[3] School of Electrical Engineering and Computer Science, University of Ottawa, Ottawa, ON K1N 6N5, Canada
petriu@uottawa.ca

Abstract: The first goal of this paper is to obtain the optimal models of nonlinear processes represented by vertical three-tank systems. This paper also presents the design of optimal sliding mode and super-twisting sliding mode controllers employed for controlling the liquid level in the first tank of the vertical three-tank systems. An optimization problem is defined in order to ideally minimize and practically reduce the differences between the outputs of the laboratory equipment for real-time experiments and the outputs of the nonlinear models. Therefore, the parameters of the nonlinear models and of the proposed controllers are optimally tuned using a recent metaheuristic optimization algorithm, namely the Grey Wolf Optimizer (GWO), which solves six optimization problems. The objective functions are defined as the sums of the squared control errors, and they are solved in the iteration domain by also using a GWO algorithm. Comparative analyses of the responses of the laboratory equipment for real-time experiments and of the derived optimal nonlinear models are carried out in various simulation scenarios. The control structures are also validated through simulations and real-time experiments. The simulation and the experimental results prove that the performance of the control systems improves after ten iterations of the GWO algorithms.

Keywords: Sliding mode control, Super-twisting sliding mode control, Grey wolf optimizer, Vertical three-tank systems.

1. Introduction

In order to control the liquid level in the nonlinear three-tank systems some recent control structures are detailed in the following: the Proportional-Integral-Derivative (PID) control (Hedrea et al., 2019), fuzzy control including stability analysis (Precup et al., 2013) and accounting for multi input-multi output structures (Bojan-Dragos et al., 2019), switched model predictive control (Mirzaee & Salahshoor, 2012), robust and fuzzy predictive control (Bouzouita et al., 2008), gain-scheduling control in combination with linear controllers (Chakravarthi et al., 2014) and focusing on Proportional-Integral (PI) controllers (Dinesh Kumar & Meenakshipriya, 2012), sliding mode control with fault diagnosis (Orani et al., 2009) nonlinear sliding surface (Boubakir et al., 2009) and secong-order or second order sliding mode control (Bartolini et al., 1999) with robust performance (Khalid & Spurgeon, 2006). The convenient and relatively simple design of optimal discretized linear and nonlinear controllers for multi-input multi-output nonlinear three-tank systems is based on the Jacobian linearization of these nonlinear system models. The controllers are then validated using the Automatic Control and Dynamic Optimization (ACADO) toolbox introduced in the study of Emebu et al. (2023). In (Meng et al., 2022), a feedback linearization technique is introduced for a quadruple-tank liquid level system, utilizing a nonlinear disturbance observer. In order to address the challenges posed by the nonlinearities of mathematical models in vertical three-tank systems, system model uncertainties, process delays, and disturbances in industrial applications, the development of a robust control strategy with sliding mode controllers is motivated in (Shah & Patel, 2019). A comprehensive analysis of sliding mode and super-twisting sliding mode control in a three-tank system can be found in the works of Hosokawa et al. (2023) and Almutairi & Zribi (2006). The implementation of such control systems can effectively mitigate the impact of uncertainties in the multi-tank system model and alleviate the issue of chatter phenomenon. A self-controling and resilient control system, utilizing an optimal fuzzy sliding mode controller, was developed by Delavari et al. (2010) for a nonlinear coupled

https://doi.org/10.24846/v33i3y202401 ICI Bucharest © Copyright 2012-2024. All rights reserved

tanks system. A control approach using a neuro-fuzzy-sliding mode controller is presented in (Boubakir et al., 2009) to deal with the chattering issue and handle the challenge of equivalent control computation in a connected tank system.

The papers by Khalid & Spurgeon (2006) and Orani et al. (2010) demonstrate that the implementation of a second-order sliding mode control method leads to the enhancement of certain performance metrics in robust control solutions. A second-order sliding mode control algorithm is proposed in (Khalid & Spurgeon, 2006) to control the liquid level in interconnected twin-tanks and adapt to parameter changes such as tank area, admittance coefficients of different pipes, tank leakage, and pump dynamics variability. Orani et al. (2010) developed an observer with a corrective term based on a second-order sliding mode control algorithm for fault diagnosis and disturbance observation in a hydraulic vertical three-tank system.

The advantage of the second-order sliding mode control consists in the fact that is proved to behave more efficiently in controlling the uncertain nonlinear systems than the classical sliding mode control due to very simple control laws and due to the ensuring of an improvement of the sliding precision with respect to classical sliding mode control (Bartolini et al., 1999), while the disadvantage of using second-order sliding mode controllers consists in the fact that the tuning of their parameters depends on the bounds of the uncertain dynamics and on the chosen sliding manifold.

Taking this into consideration, the development of sliding mode and super-twisting sliding mode controllers for vertical three-tank systems is motivated and discussed in this paper.

Optimal parameter adjustment of a nonlinear vertical three-tank system model is the main contribution of this work. The optimization problem is tackled using a Grey Wolf Optimization (GWO) algorithm, which aims to minimize the objective function represented as the mean value of the squared modeling errors. The comparative evaluations demonstrate that the proposed models are a crucial approach in obtaining models with a high level of accuracy.

The second contribution is the formulation of optimization problems aimed at enhancing the efficiency of the suggested control systems. These problems take into account the objective functions as the sums of squared control errors and the variables as the fitting parameters of the sliding mode controllers. Optimization difficulties are addressed using Grey Wolf Optimization (GWO) algorithms to precisely adjust the parameter settings of the proposed controllers.

The third contribution of this paper is the development and validation of a sliding mode control structure and of a super-twisting sliding mode control structure for liquid level control of a nonlinear vertical three-tank system. This is validated through simulation and laboratory experimentation. The motivation behind the development of the suggested controllers is their straightforward design and practical use in industrial settings. First, a control solution is designed to minimize chattering. Second, a Super-Twisting Sliding Mode (STSM) controller is combined with a Proportional Plus Integral (PPI) controller to cancel out the switching variable in specific steady-state regimes and maintain the necessary steady-state regime for system performance with regard to the reference input.

This paper is organized in the following manner. The analysis of optimization issues addressed by GWO algorithms is detailed in Section 2. Section 3 establishes the appropriate models for the nonlinear process of the vertical three-tank system. Section 4 provides a comprehensive explanation of the theoretical design support for control solutions, namely the sliding mode PI controller and Super-Twisting Sliding Mode controller paired with the PPI controller. Additionally, this section presents the tuning parameters of the employed algorithms. The proposed optimal controllers are verified through the analysis of several scenarios in Section 5. Section 6 outlines the conclusions and future research directions.

2. Optimization Problems and Algorithms

To obtain the optimal parameters of the nonlinear model of the vertical three-tank system, the following optimization problem is involved:

$$\begin{aligned}\boldsymbol{\rho}^{(j)*} &= \arg\min_{\boldsymbol{\rho}^{(j)}\in D_{\boldsymbol{\rho}}} J_M(\boldsymbol{\rho}^{(j)}),\ J_M(\boldsymbol{\rho}^{(j)}) = \frac{1}{L}\sum_{k=1}^{L} e_{M,k}^2(\boldsymbol{\rho}^{(j)}) \\ &= \frac{1}{L}\sum_{k=1}^{L}[y_k^*(\boldsymbol{\rho}^{(j)}) - y_k(\boldsymbol{\rho}^{(j)})]^2,\end{aligned} \tag{1}$$

where j symbolizes the model, $e_{M,k}(\boldsymbol{\rho}^{(j)}) = y_k^*(\boldsymbol{\rho}^{(j)}) - y_k(\boldsymbol{\rho}^{(j)})$ symbolizes the modeling error at k^{th} sampling interval, $y_k^*(\boldsymbol{\rho}^{(j)})$ represents the real system output, $y_k(\boldsymbol{\rho}^{(j)})$ represents the model output, $\boldsymbol{\rho}^{(j)}$ represents the model parameter vector, $\boldsymbol{\rho}^{(j)*}$ represents the optimal model parameter vector, D_{ρ} marks the feasible domain of $\boldsymbol{\rho}^{(j)}$, and L marks the length of the discrete time horizon. The objective function $J_M(\boldsymbol{\rho}^{(j)})$ is a metric used to evaluate the model performance.

To obtain the optimal parameters of the controllers, the following optimization problem is involved:

$$\begin{aligned}\boldsymbol{\rho}^{(j)*} &= \arg\min_{\boldsymbol{\rho}^{(j)}\in D_{\rho}} J_C(\boldsymbol{\rho}^{(j)}), J_C(\boldsymbol{\rho}^{(j)}) = \frac{1}{L}\sum_{k=1}^{L} e_{C,k}^2(\boldsymbol{\rho}^{(j)}) \\ &= \frac{1}{L}\sum_{k=1}^{L}[r_k^*(\boldsymbol{\rho}^{(j)}) - y_k(\boldsymbol{\rho}^{(j)})]^2,\end{aligned} \tag{2}$$

where j symbolizes the controller, $e_{C,k}(\boldsymbol{\rho}^{(j)}) = r_k(\boldsymbol{\rho}^{(j)}) - y_k(\boldsymbol{\rho}^{(j)})$ symbolizes the control error at k^{th} sampling interval, $y_k^*(\boldsymbol{\rho}^{(j)})$ symbolizes the reference input or set-point, $r_k(\boldsymbol{\rho}^{(j)})$ symbolizes the controlled output, $\boldsymbol{\rho}^{(j)}$ symbolizes the controller parameter vector, $\boldsymbol{\rho}^{(j)*}$ symbolizes the optimal controller parameter vector, and, similarly to equation (1), D_{ρ} marks the feasible domain of $\boldsymbol{\rho}^{(j)}$, and L the length of the discrete time horizon. The objective function $J_C(\boldsymbol{\rho}^{(j)})$ is a metric used to evaluate the control system performance and thus the controller performance.

The GWO algorithm, as documented in the easily understandable formulations in the works of Precup et al. (2016) and Bojan-Dragos et al. (2021), begins by prioritizing the initialization of the agents, namely the wolves or solution candidates. Every agent of the total of N agents is represented by its position vector $\boldsymbol{X}_i(\mu) \in R^q$, which is defined by the following statement:

$$\mathbf{X}_i(\mu) = [x_i^1(\mu) \ldots x_i^f(\mu) \ldots x_i^q(\mu)]^T, \; i = 1 \ldots N, \tag{3}$$

where $x_i^f(\mu)$ is the position of i^{th} agent in f^{th} dimension, $f = 1...q$, μ is the current iteration index, $\mu = 1...\mu_{\max}$, $\mu_{\max}$ is the maximum number of iterations, and q is the dimension of the search space, and also denotes the number of variables of the model and of each controller as well. Additional details on GWO algorithms and their specific vector operations are described in (Precup et al., 2016; Precup et al., 2020).

The GWO algorithm is used to solve the optimization problems specified in equations (1) and (2) in terms of the following mappings:

$$\begin{aligned}&\boldsymbol{\rho}^{(j)} = \mathbf{X}_i(\mu) \subset D_{\rho}, \;\; i = 1...N, \\ &\boldsymbol{\rho}^{(j)*} = \arg\min_{i=1...N} J(\mathbf{X}_i(\mu_{\max})),\end{aligned} \tag{4}$$

with $j \in \{\text{LnM, SM-C, STSM-PPI-C}\}$, where LnM marks a proportional with a second-order low-pass filter-controller, STSM-PPI-C is a controller that combines a STSM controller with a PPI controller, and $p \in \{M, C\}$, where M marks the process model, and C marks the controller.

The optimization procedure outlined in this section is viewed as a procedure to train a model. The optimization problems provided in equations (1) and (2) are employed to optimize the parameter values of a nonlinear model of a vertical three-tank system and the controllers.

3. Process Model

The vertical three-tank system (V3TS) laboratory equipment, as shown in Figure 1 (Inteco, 2007), will be used in the following as a controlled process. This equipment was installed in one of the laboratories of the Politehnica University of Timisoara, Romania, called Intelligent Control Systems Laboratory.

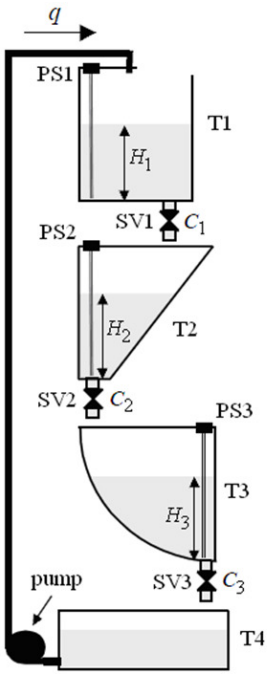

Figure 1. The block diagram of the vertical three-tank system laboratory equipment, adapted from (Inteco, 2007)

The process comprises three vertically positioned tanks (T1, T2 and T3) and one tank (T4) positioned below the lower tank (T3) acting as a reflux tank. A pump driven by a DC motor

ICI Bucharest © Copyright 2012-2024. All rights reserved

supplies water to tank T1, while three electrical servo valves (SV1, SV2 and SV3) control the outflow from each tank. Piezo-resistive pressure sensors PS1, PS2 and PS3 measure the water levels in tanks H_1, H_2, and H_3, respectively.

The first-principles state-space equations of the process are (Inteco, 2007):

$$\begin{aligned}
&\dot{H}_1 = q/\beta_1(H_1) - R_1 H_1^{\alpha_1}/\beta_1(H_1),\\
&\dot{H}_2 = R_1 H_1^{\alpha_1}/\beta_1(H_2) - R_2 H_2^{\alpha_2}/\beta_2(H_2),\\
&\dot{H}_3 = R_2 H_2^{\alpha_2}/\beta_2(H_3) - R_3 H_3^{\alpha_3}/\beta_3(H_3),\\
&y_{H1} = H_1, y_{H2} = H_2, y_{H3} = H_3,
\end{aligned} \tag{5}$$

where $q = k_{EE}u$ is the inflow in time, u is the control input of the first tank, $k_{EE} = 1.6 \cdot 10^{-4}$, H_i, $i = 1,3$, is the fluid level of the i^{th} tank, α_i, $i = \overline{1,3}$, is the flow coefficient for the i^{th} tank, R_i, $i = \overline{1,3}$, is the resistance of the output orifice of i^{th} tank, $\beta_i(H_i)$, $i = \overline{1,3}$, is the cross sectional area of i^{th} tank computed at the level H_i, and y_{Hi}, $i = \overline{1,3}$ is the measured fluid level.

The parameters have the following numerical values: $R_1 = 11.08 \cdot 10^{-5}$, $R_2 = 8.78 \cdot 10^{-5}$, $\alpha_1 = \alpha_2 = 0.5$, $a_H = 0.25$, $b_H = 0.345$, $c_H = 0.1$, $w = 0.035$, $q = 0.435 \cdot 10^{-4}$, $H_{1max} = H_{2max} = H_{3max} = 0.35$.

Measurements were conducted in real time on the vertical three-tank system equipment, and a single input-output dataset was maintained. In this paper, the input data used, namely u – the control signal applied to the first tank, is depicted in Figure 2. Additionally, Figure 3 illustrates the output signal, H_1, which represents the fluid level in the first tank.

This input-output dataset will be used in the comparative analysis conducted in this paper. Alternative input-output datasets were used for both training and testing in this work.

A first comparison illustrated in Figure 4 was made between the responses of the nonlinear mathematical model of the vertical three-tank system with the parameters given by Inteco (2007) and the vertical three-tank system laboratory equipment. The major differences observed between them justify one of the aims of this paper, that is to obtain the optimal parameters of the nonlinear model in equation (5).

In order to achieve optimal performance and avoid becoming trapped in a local minimum,

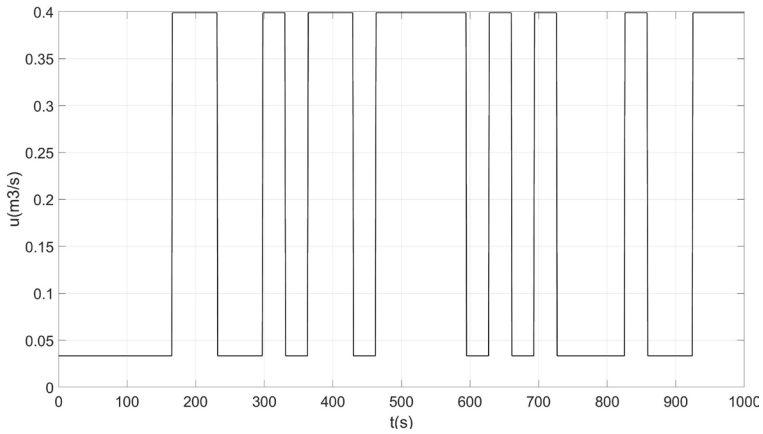

Figure 2. The block diagram of the vertical three-tank system laboratory equipment (Inteco, 2007)

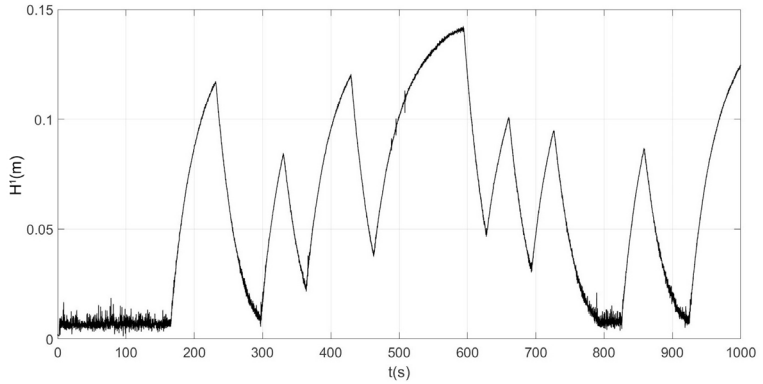

Figure 3. The block diagram of the vertical three-tank system laboratory equipment (Inteco, 2007)

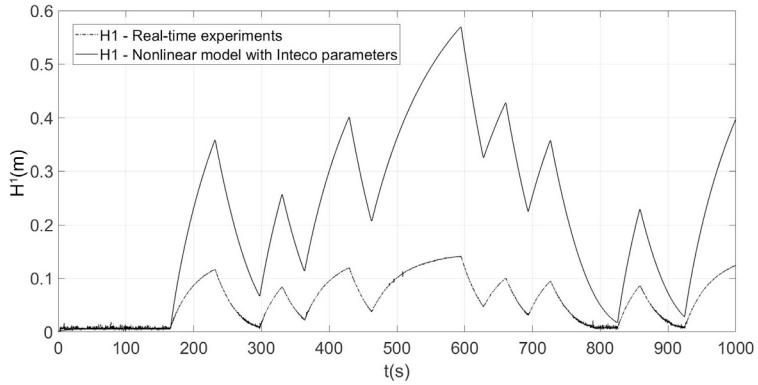

Figure 4. The block diagram of the vertical three-tank system laboratory equipment (Inteco, 2007)

the GWO algorithms were configured with the following variables: $N = 100$ agents and $\mu_{max} = 100$ iterations. Ten iterations of the GWO algorithms were performed for each optimization scenario, and the outcomes are shown below after their subsequent averaging.

The parameter vector of the vertical three-tank system model used in this paper is

$$\boldsymbol{\rho}^{(1)} = [k_{EE} \quad R_1 \quad R_2 \quad \alpha_1 \quad \alpha_2 \quad a_H \quad b_H \quad c_H \quad w \quad H_{2max}]^T, \tag{6}$$

where T indicates matrix transposition.

Solving the optimization problem in equation (1) with GWO algorithm while considering the parameter intervals $k_{EE} \in [0.85 \cdot 10^{-4}, 1.5 \cdot 10^{-4}]$, $R_1 \in [0.1 \cdot 10^{-3}, 0.2 \cdot 10^{-3}]$, $R_2 \in [0.75 \cdot 10^{-4}, 0.95 \cdot 10^{-4}]$, $\alpha_1 \in [0.35, 0.55]$, $\alpha_2 \in [0.5, 0.6]$, $a_H \in [0.2, 0.4]$, $b_H \in [0.2, 0.5]$, $c_H \in [0.5, 0.3]$, $w \in [0.3, 0.5]$, and $H_{2max} \in [0.1, 0.4]$, the optimal parameter vector is derived as:

$$\boldsymbol{\rho}^{(1)*} = [0.94 \cdot 10^{-4} \quad 0.113 \cdot 10^{-3} \quad 0.85 \cdot 10^{-4} \quad 0.44 \quad 0.55 \quad 0.28 \quad 0.35 \quad 0.115 \quad 0.036 \quad 0.348]^T \tag{7}$$

The controllers described below are designed by identifying the dynamic characteristics of a vertical three-tank system as a second-order low-pass filter linear model (LnM) with the transfer function:

$$H_{V3TS}(s) = \frac{y_{H_1}(s)}{u(s)} = k_{CP} / [(1 + T_1 s)(1 + T_2 s)], \tag{8}$$

where the parameters are optimally tuned by using a GWO algorithm.

The parameter vector of this mathematical model is:

$$\boldsymbol{\rho}^{(2)} = [k_{PC} \quad T_1 \quad T_2]^T \tag{9}$$

Solving the optimization problem defined in equation (1) with GWO algorithm while considering the parameter intervals $k_{CP} \in [0.2, 0.3]$, $T_1 \in [30, 40]$, $T_2 \in [0.1, 1]$, the optimal parameter vector of the model is derived as:

$$\boldsymbol{\rho}^{(2)*} = [0.23 \quad 34 \quad 0.41]^T \tag{10}$$

4. Control System Structure and Design Approach

4.1 Sliding Mode Controller

The structure of the control system with sliding mode controller is given in Figure 5 and the tuning parameters are $T_i > 0$, $\alpha > 0$ and $c > 0$. The control law is:

$$u(t) = \psi(t) x_1(t) + \frac{1}{T_i} \int_0^t \psi(\tau) x_1(\tau) d\tau, \tag{11}$$

where the nonlinear switching term is:

$$\psi(t) = \alpha \, \mathrm{sgn}(\sigma(t) x_1(t)), \; x_1(t) = e(t) \tag{12}$$

The sliding mode controller (SM-C) parameters are adjusted using three types of tuning approaches. In the *first* one, three steps are used to obtain the tuning parameters:

Step 1. Aiming the reduction of the settling time of the control system, the integral time constant, $T_i = 18.7$ s, is established.

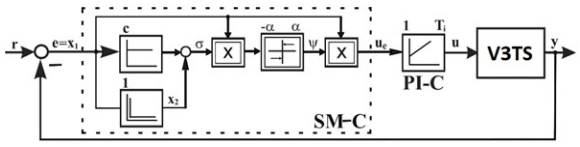

Figure 5. Sliding mode control system structure

Step 2. The switching variable $\sigma(t)$ is defined as:

$$\sigma(t) = c \, x_1(t) + x_2(t), \tag{13}$$

ICI Bucharest © Copyright 2012-2024. All rights reserved

where $c = 2.32 < a_2$, $c > 0$ will be selected to achieve the certain behaviors of the control system on the sliding manifold.

The equations describing the state-space of the closed-loop system are:

$$\begin{aligned} \dot{x}_1(t) &= x_2(t), \\ \dot{x}_2(t) &= -a_1 x_1(t) - a_2\, x_2(t) + b\, u(t) + f(t), \end{aligned} \tag{14}$$

where a_1, a_2, b and f are constant parameters with the expressions:

$$a_1 = \frac{6}{T_1 T_2}, a_2 = 5\frac{T_1 + T_2}{T_1 T_2}, b = -\frac{k_b}{T_1 T_2}, f = \frac{0.35}{T_1 T_2}, \tag{15}$$

and the following numerical values:

$$\begin{aligned} &a_1 = 10.76,\ a_2 = 24.3,\ b = 2.44 \\ &f = 0.056,\ c = 18.23 \end{aligned} \tag{16}$$

Step 3. The sliding mode reaching and existence requirement, that is:

$$\sigma(t)\,\dot{\sigma}(t) < 0 \tag{17}$$

is proved by taking into account the global asymptotic stabilization required by Lyapunov's stability theory, $\dot{V}(t) < 0$, using the Lyapunov function candidate solution $V(t) = 0.5\sigma^2(t)$.

By differentiating equation (13) and substituting $x_2(t) = \sigma(t) - \mathrm{c}x_1(t)$ with $\dot{\sigma}(t)$, the condition for the existence of equation (17) is derived:

$$\begin{aligned} \sigma(t)\dot{\sigma}(t) = -\sigma(t)\,[(a_1 + c^2 - a_2 c)x_1(t) - bu(t) - f] \\ + (c - a_2)\sigma^2(t)\ < 0 \end{aligned} \tag{18}$$

Due to condition $c < a_2$, the term $(\mathrm{c} - a_2)\sigma^2(t)$ in (18) is usually negative, so to obtain equation (17) a sufficient condition is:

$$\sigma(t)\,[(a_1 + c^2 - a_2 c)x_1(t) - bu(t) - f] > 0 \tag{19}$$

Substituting equations (11) and (12) in equation (19) gives:

$$\begin{aligned} &\sigma(t)\,[(a_1 + c^2 - a_2 c)x_1(t) - b\alpha x_1(t)\,\mathrm{sgn}(\sigma(t)x_1(t)) \\ &+ \frac{b\alpha}{T_i}\int_0^t x_1(\tau)\,\mathrm{sgn}(\sigma(\tau)x_1(\tau))d\tau - f] > 0 \end{aligned} \tag{20}$$

Under the conditions of Lyapunov's stability theory, the sign of $\sigma(t)$ in (20) is discussed in the following. In the first case with $\sigma(t) > 0$ the equation (20) becomes:

$$\begin{aligned} &(a_1 + c^2 - a_2 c)x_1(t) - b\alpha x_1(t)\,\mathrm{sgn}(\sigma(t)x_1(t) \\ &+ \frac{b\alpha}{T_i}\int_0^t x_1(\tau)\,\mathrm{sgn}(\sigma(\tau)x_1(\tau)\ d\tau - f(t) > 0, \end{aligned} \tag{21}$$

and (21) is reorganized leading to:

$$b\alpha < \frac{(a_1 + c^2 - a_2 c)x_1(t) - f(t)}{|\,x_1(t)\,| + \frac{1}{T_i}\int_0^t |\,x_1(\tau)\,|\,d\tau} \tag{22}$$

In the second case with σ(t) < 0 the equation (20) becomes:

$$\begin{aligned} &(a_1 + c^2 - a_2 c)x_1(t) - b\alpha x_1(t)\,\mathrm{sgn}(\sigma(t)x_1(t) \\ &+ \frac{b\alpha}{T_i}\int_0^t x_1(\tau)\,\mathrm{sgn}(\sigma(\tau)x_1(\tau)\ d\tau - f(t) < 0, \end{aligned} \tag{23}$$

and (23) is reorganized leading to:

$$b\alpha < -\frac{(a_1 + c^2 - a_2 c)x_1(t) - f(t)}{|\,x_1(t)\,| + \frac{1}{T_i}\int_0^t |\,x_1(\tau)\,|\,d\tau} \tag{24}$$

The condition necessary to confidently ensure the sliding mode reaching and existence condition is derived from equations (22) and (24):

$$b\alpha < -\frac{|\,(a_1 + c^2 - a_2 c)x_1(t) - f(t)\,|}{|\,x_1(t)\,| + \frac{1}{T_i}\int_0^t |\,x_1(\tau)\,|\,d\tau} \tag{25}$$

The *second* approach involves tuning the parameters T_i, a_1, a_2, b, f and $c > 0$ using the proposed optimization algorithm with the following parameter vector:

$$\boldsymbol{\rho}^{(3)} = [T_i \quad a_1 \quad a_2 \quad b \quad f \quad c\,]^T \tag{26}$$

Solving the optimization problem defined in equation (2) with GWO algorithm while considering the parameter intervals $T_i \in [10, 100]$, $a_1 \in [0.06, 0.08]$, $a_2 \in [2, 3]$, $b \in [-0.5, -0.4]$, $f \in [0.001, 0.002]$, and $c \in [1, 3]$, the optimal parameter vector of the model is derived as:

$$\boldsymbol{\rho}^{(3)*} = [16.08\ \ 0.07\ \ 2.46\ \ -0.49\ \ 0.0014\ \ 2.2]^T \tag{27}$$

The *third* approach involves tuning the parameters $T_i > 0$, $\alpha > 0$ and $c > 0$ using the proposed optimization algorithm with the following parameter vector:

$$\boldsymbol{\rho}^{(4)} = [T_i \quad \alpha \quad c]^T \tag{28}$$

Solving the optimization problem defined in equation (2) with GWO algorithm while considering the parameter intervals $T_i \in [10, 100]$, $\alpha \in [0.1, 1]$, $c \in [1, 3]$, the vector containing the optimal parameter vector of the controller is derived as:

$$\boldsymbol{\rho}^{(4)*} = [25.6 \quad 0.91 \quad 1.99]^T \tag{29}$$

4.2 Super-Twisting Sliding Mode Controller

In the sliding mode control theory, the controllers that exhibit STSM are classified as second-order sliding controllers. The abovementioned controllers have the capability to control second-order systems and effectively prevent chattering. Proposed by Levant in (Levant, 2003; Levant, 2005; Levant, 2007), STSM controllers were successfully applied to electrical drives in (Lascu et al., 2013). The fundamental concept of this controller is to subject the switching action to the higher-order derivatives of the control signal, rather than to its first derivative as seen in the case of SM-C. Therefore, the control signal converges to the corresponding control, so it avoids the presence of noise. The stability of such control systems must be proved as indicated in the studies conducted by Levant (2005) and Lascu et al. (2013).

Figure 6 illustrates the structural framework of the control system with STSM controller, with the tuning parameters $T_i > 0$, $\alpha > 0$ and $c > 0$.

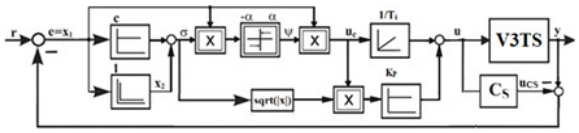

Figure 6. Super-twisting sliding mode control system structure

The control law is derived from (Lascu et al., 2013):

$$u(t) = K_P\sqrt{|x_1(t)|}\psi(t)x_1(t) + \frac{1}{T_i}\int_0^t \psi(t)x_1(\tau)d\tau, \qquad (30)$$

where the nonlinear switching term is:

$$\begin{aligned} &\psi(t) = \alpha\,\mathrm{sgn}(\sigma(t)x_1(t)),\\ &x_1(t) = e(t),\ K_P = 1. \end{aligned} \qquad (31)$$

This paper described three different approaches for tuning the parameters of the super-twisting sliding mode controller (STSM-PPI-C).

The *first* approach mimics the design procedures of SM-C to derive the tuning parameters. In the *first* step, the integral time constant, T_i = 34 s, is established.

In *step* 2, the switching variable $\sigma(t)$ is expressed as equation (13).

In *step 3*, the analysis of the global asymptotical stabilization scenario in Lyapunov's stability theory, $\dot{V}(t) < 0$, begins with the examination of the sliding mode reaching and existence condition expressed in equation (14) and the Lyapunov function $V(t) = 0.5\sigma^2(t)$.

Performing the calculations in equations (13) to (19) and substituting equations (30) and (31) in equation (19) yields:

$$\begin{aligned} &\sigma(t)\,[(a_1 + c^2 - a_2c)x_1(t)\\ &-b\alpha\sqrt{|x_1(t)|}\,\mathrm{sgn}(\sigma(t)x_1(t))x_1(t)\\ &+\frac{b\alpha}{T_i}\int_0^t \mathrm{sgn}(\sigma(t)x_1(t))x_1(\tau)d\tau - f(t)] > 0 \end{aligned} \qquad (32)$$

Under the conditions of Lyapunov's stability theory, the sign of $\sigma(t)$ in (32) is discussed in the following. In the first case with $\sigma(t) > 0$, equation (32) becomes:

$$\begin{aligned} &(a_1 + c^2 - a_2c)x_1(t) - b\alpha\sqrt{|x_1(t)|}\,\mathrm{sgn}(\sigma(t)x_1(t))x_1(t)\\ &+\frac{b\alpha}{T_i}\int_0^t \mathrm{sgn}(\sigma(t)x_1(t))x_1(\tau)d\tau - f(t) > 0 \end{aligned} \qquad (33)$$

Equation (33) is reorganized leading to:

$$b\alpha < \frac{(a_1 + c^2 - a_2c)x_1(t) - f(t)}{|x_1(t)|\sqrt{|x_1(t)|} + \frac{1}{T_i}\int_0^t |x_1(\tau)|\,d\tau} \qquad (34)$$

In the second case, with $\sigma(t) < 0$, equation (32) becomes:

$$\begin{aligned} &(a_1 + c^2 - a_2c)x_1(t) - b\alpha\sqrt{|x_1(t)|}\,\mathrm{sgn}(\sigma(t)x_1(t))x_1(t)\\ &+\frac{b\alpha}{T_i}\int_0^t \mathrm{sgn}(\sigma(t)x_1(t))x_1(\tau)d\tau - f(t) < 0 \end{aligned} \qquad (35)$$

Equation (35) is manipulated leading to:

$$b\alpha < \frac{-(a_1 + c^2 - a_2c)x_1(t) + f(t)}{|x_1(t)|\sqrt{|x_1(t)|} + \frac{1}{T_i}\int_0^t |x_1(\tau)|\,d\tau} \qquad (36)$$

The sufficient condition to ensure the sliding mode reaching and existence condition is obtained based on equations (34) and (36):

$$b\alpha < -\frac{|(a_1 + c^2 - a_2c)x_1(t) - f(t)|}{|x_1(t)|\sqrt{|x_1(t)|} + \frac{1}{T_i}\int_0^t |x_1(\tau)|\,d\tau} \qquad (37)$$

The numerical values of the parameters of the STSM-PPI-C are obtained as:

$$\begin{aligned} &a_1 = 0.072,\ a_2 = 2.45,\ b = -0.45\\ &f = 0.0014,\ c = 2.1 \end{aligned} \qquad (38)$$

In the *second* approach, the parameters T_i, a_1, a_2, b, f and $c > 0$ are tuned using the proposed optimization algorithm with the following parameter vector:

$$\boldsymbol{\rho}^{(5)} = [T_i \quad a_1 \quad a_2 \quad b \quad f \quad c\,]^T \qquad (39)$$

ICI Bucharest © Copyright 2012-2024. All rights reserved

Solving the optimization problem defined in equation (2) with GWO algorithm while considering the parameter intervals $T_i \in [10, 100]$, $a_1 \in [0.07, 0.08]$, $a_2 \in [2, 3]$, $b \in [-0.5, -0.4]$, $f \in [0.001, 0.003]$, $c \in [1, 3]$, the parameter vector of the controller is derived as:

$$\boldsymbol{\rho}^{(5)*} = [33 \quad 0.075 \quad 2.45 \quad -0.45 \quad 0.0014 \quad 2]^T \tag{40}$$

In the *third* aproach, the parameters $T_i > 0$, $\alpha > 0$ and $c > 0$ are tuned using the proposed optimization algorithm with the following parameter vector:

$$\boldsymbol{\rho}^{(6)} = [T_i \quad \alpha \quad c]^T \tag{41}$$

Solving the optimization problem defined in equation (2) with GWO algorithm while considering the parameter intervals $T_i \in [10, 100]$, $\alpha \in [0.9, 1]$, and $c \in [1, 3]$, the parameter vector of the controller is derived as:

$$\boldsymbol{\rho}^{(6)*} = [43.3 \quad 0.95 \quad 1.95]^T \tag{42}$$

5. Simulation and Experimental Results

The design methodology and control approaches were verified by simulations and real-time experiments conducted on laboratory equipment for the vertical three-tank system briefly described in Section 3. The experimental configuration was depicted in Figure 1.

All optimization analyses in this work were conducted using a simulation scenario with a time horizon of 1000 seconds and a sampling period of 0.01. Ten iterations of the GWO algorithms were executed, resulting in the following results collected after their averaging.

Figure 7 illustrates a comparison between the fluid level in the first tank of the nonlinear model, using the optimal parameters identified in equation (7), and the fluid level in the first tank of the laboratory equipment for real-time experiments. The measured value of the objective function in the nonlinear model determined by the optimal parameters is $J_M(\boldsymbol{\rho}^{(1)}) = 5.85 \cdot 10^{-5}$.

Figure 8 shows a comparison between the fluid level in the first tank of the linear model, which has the optimal parameters identified in equation (10), and the fluid level in the first tank of the laboratory equipment for real-time experiments. The observed value of the objective function

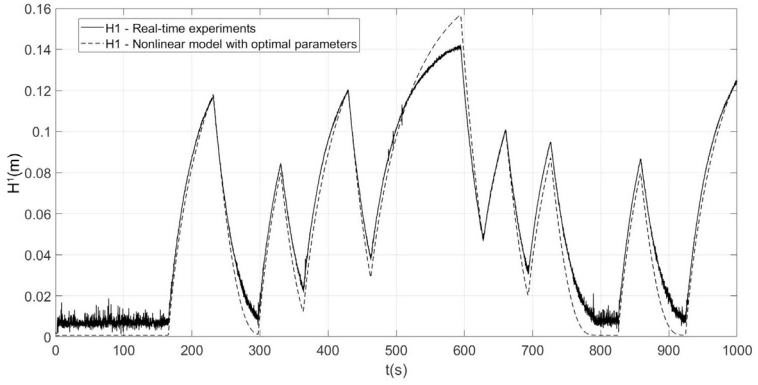

Figure 7. Responses of the vertical three-tank system laboratory equipment and of the nonlinear model with the optimal parameters given in equation (7)

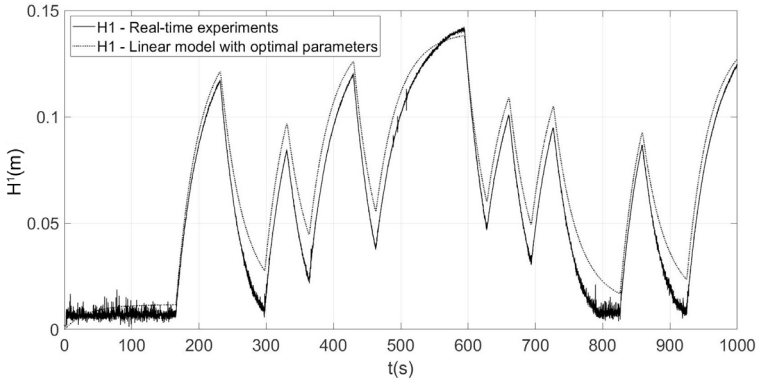

Figure 8. Responses of the vertical three-tank system laboratory equipment and of the linear model with the optimal parameters given in equation (10)

in the linear model determined by the optimal parameters is $J_M(\boldsymbol{\rho}^{(2)}) = 1.29 \cdot 10^{-4}$.

Figure 9 displays the graph representation of the response of the nonlinear model using parameters from (Inteco, 2007), the response of the nonlinear model with the optimal parameters specified in equation (7), the response of the linear model with the optimal parameters specified in equation (10), and the real-time response of the equipment.

Other comparisons were carried out considering the control systems with SM-C and STSM-PPI-C designed above which were tested by digital simulations and by real-time experiments on the nonlinear vertical three-tank system laboratory equipment.

The further comparisons depicted in Figures 10-13 given in (Bojan-Dragos et al., 2024) were conducted by simulation or real-time tests to compare the controlled response of SM-C with the parameters derived from the approaches outlined in Section 4.

Figure 10 given in (Bojan-Dragos et al., 2024) displays the control signal u (m3/s) and the fluid level in the first tank, H_1 (m), shown as a function of time, t(s), produced by simulation for SM-C with the parameters specified in equation (16) and for CS with SM-C with the optimal values specified in equation (27). The measured value of the objective function in the CS framework with SM-C, considering the optimal parameters, is $J_c(\boldsymbol{\rho}^{(3)}) = 2.65 \cdot 10^{-4}$.

Figure 11 given in (Bojan-Dragos et al., 2024) displays the control signal u (m3/s) and the liquid level in the first tank, H_1 (m), derived from real-time experiments for SM-C with the parameter values specified in equation (16) and for CS with SM-C with the optimal parameters as shown in equation (27).

Figure 12 given in (Bojan-Dragos et al., 2024) displays the control signal u (m3/s) and the fluid level in the first tank, H_1 (m), obtained from simulation and real-time experiments in the case of SM-C with the optimal parameters specified in equation (16).

The time-dependent control signal u (m3/s) and the fluid level in the first tank, H_1 (m), derived from simulation and real-time experiments in the case of CS with SM-C with the optimal parameters specified in equation (27) are shown in Figure 13 given in (Bojan-Dragos et al., 2024).

The results related to the behavior of the SM-C are illustrated in terms of system responses with the parameters specified in equation (29). In the case of CS with SM-C, the measured value of the objective function with the optimal parameters is $J_c(\boldsymbol{\rho}^{(4)}) = 4.22 \cdot 10^{-4}$. Figure 14 given in (Bojan-Dragos et al., 2024) displays the control signal u (m3/s) and the fluid level in the first tank, H_1 (m), derived from digital simulation and real-time measurements.

The further comparisons depicted in Figures 15-18 given in (Bojan-Dragos et al., 2024) were conducted by simulation or real-time tests to compare the controlled response of STSM-PPI-C with the parameters derived from the approaches proposed in Section 4.

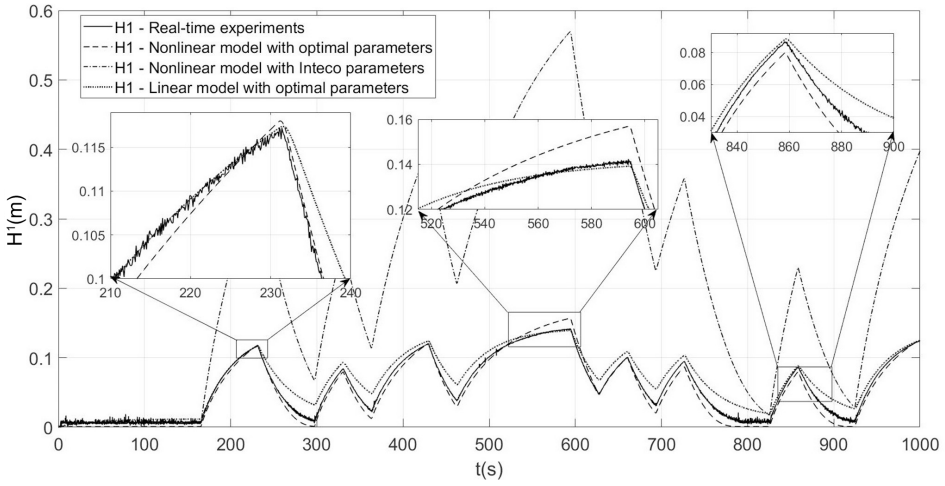

Figure 9. Responses of the vertical three-tank system laboratory equipment, the nonlinear model in equation (5) with the parameters given by Inteco (2007), the nonlinear model in equation (5) with the optimal parameters and of the linear model with the optimal parameters specified in equation (10)

ICI Bucharest © Copyright 2012-2024. All rights reserved

Figure 15 given in (Bojan-Dragos et al., 2024) displays the control signal u (m3/s) and the fluid level in the first tank, H_1 (m), over time, $t(s)$, obtained by simulation for STSM-PPI-C with the parameters specified in equation (38) and for CS with STSM-PPI-C with the optimal parameters specified in equation (40). The value of the objective function obtained in this comparison is $J_c(\boldsymbol{\rho}^{(5)}) = 2.31 \cdot 10^{-4}$.

Figure 16 given in (Bojan-Dragos et al., 2024) displays the control signal u (m3/s) and the fluid level in the first tank, H_1 (m), obtained from real-time experiments. The analysis was conducted for both CS with STSM-PPI-C with the parameters specified in equation (38) and CS with STSM-PPI-C with the optimal parameters specified in equation (40).

Figure 17 given in (Bojan-Dragos et al., 2024) displays the control signal u (m3/s) and the fluid level in the first tank, H_1 (m), obtained from simulation and real-time experiments for STSM-PPI-C with the optimal parameters specified in equation (38).

Figure 18 given in (Bojan-Dragos et al., 2024) depicts the control signal u (m3/s) and the fluid level in the first tank, H_1 (m), obtained from simulation and real-time experiments in the case of CS with STSM-PPI-C with the optimal parameters specified in equation (40).

The following results include the responses of the STSM-PPI-C with the parameters specified in equation (42). The measured value of the objective function in the CS approach using STSM-PPI-C with the optimal parameters is $J_c(\boldsymbol{\rho}^{(6)}) = 2.33 \cdot 10^{-4}$. Figure 19 given in (Bojan-Dragos et al., 2024) depicts the evolution of the control signal u (m3/s), and the fluid level in the first tank, H_1 (m), over time, t (s), as measured by digital simulation and real-time tests.

Tables 1 to 3 given in (Bojan-Dragos et al., 2024) present synthetically the performance indices of the control structures developed in this paper, specifically focusing on settling time, rise time, and overshoot. These indices are examined for the staircase type reference signal.

The results given in Tables 1 to 3 emphasize the capacity of the proposed control structures for successfully tracking difficulties associated with complex processes.

In future improvements, these performance metrics could be enhanced by incorporating modern optimization algorithms.

Nevertheless, the conclusions are expected to vary if other applications are accounted for. Examples of such applications include servo systems (Preitl & Precup, 1996), series electric vehicles (Johanyak, 2017), mobile robots and multi-agent systems (Klancar & Blazic, 2019; Vascak et al., 2016), human well-being and resilience (Filip, 2021), permanent magnet synchronous motors (Hirpara, 2022), telesurgical robots (Precup et al., 2012), parallel processing and bio-inspired computing (Bejinariu et al., 2014), drilling (Haber-Haber et al., 2007), bin packing (Romero et al., 2023), for piezoelectric active laminated shells (Milić et al., 2023), casting processes (Radiša et al., 2017), bed combustion processes (Ćojbašić et al., 2011), friction compensation in haptic interfaces (Ando et al., 2002), complex planetary gearboxes (Vrcan et al. 2024), and natural language processing (Chen et al., 2023).

6. Conclusion

This study presents the development of sliding mode control structures and super-twisting sliding mode control structures for the purpose of controlling the fluid levels of vertical three-tank systems. For the sake of simplicity a single input-single output control system structure was considered, with the focus on the fluid level control in the first tank of this nonlinear system. Simulations and real-time experiments on the nonlinear equipment were carried out to test these control systems.

Performance indices, showing that the developed control solutions ensure zero steady-state control error, a low settling time, and no chattering, were obtained by synthesizing and analyzing the control system responses in terms of the cost function values.

In order to enhance the performance metrics of the control system, future research will focus on expanding the current work by designing control systems with sliding mode Takagi-Sugeno fuzzy controllers and super-twisting sliding mode Takagi-Sugeno fuzzy controllers.

Acknowledgements

This research was funded by grants of the Romanian Ministry of Education and Research, CNCS-UEFISCDI, project number PN-III-P4-ID-PCE-2020-0269, within PNCDI III, and NSERC from Canada.

REFERENCES

Almutairi, N. B. & Zribi, M. (2006) Sliding Mode Control of Coupled Tanks. *Mechatronics*. 16(7), 427-441. doi: 10.1016/j.mechatronics.2006.03.001.

Ando, N., Szemes, T., Korondi, P. & Hashimoto, H. (2002) Friction Compensation for 6DOF Cartesian Coordinate Haptic Interface. In: *Proceedings of 2002 IEEE/RSJ International Conference on Intelligent Robots and Systems, 30 September - 4 October 2002, Lausanne, Switzerland*. IEEE. pp. 2893-2898.

Bartolini, G., Ferrara, A., Levant, A. & Usai, E. (1999) On Second Order Sliding Mode Controllers. In: Young, K. & Özgüner, Ü. (eds.) *Variable Structure Systems, Sliding Mode and Nonlinear Control*. (*Lecture Notes in Control and Information Sciences*, vol 247). London, Springer, pp. 329-350.

Bejinariu, S. I., Costin, H., Rotaru, F., Nita, C., Luca, R. & Lazar, C. (2014) Parallel Processing and Bio-inspired Computing for Biomedical Image Registration. *Computer Science Journal of Moldova*, 22(2), 253-277.

Boubakir, A., Boudjema, F. & Labiod, S. (2009) A Neuro-fuzzy-sliding Mode Controller Using Nonlinear Sliding Surface Applied to the Coupled Tanks System. *International Journal of Automation and Computing*. 6, 72-80. doi: 10.1007/s11633-009-0072-0.

Bojan-Dragos, C.-A., Hedrea, E.-L., Precup, R.-E., Szedlak-Stînean, A.-I. & Roman, R.-C. (2019) MIMO Fuzzy Control Solutions for the Level Control of Vertical Two Tank Systems. In: *Proceedings of 16th International Conference on Informatics in Control, Automation and Robotics, 29-31 July 2019, Prague, Czech Republic*. pp. 810-817.

Bojan-Dragos, C.-A., Precup, R.-E., Petriu, E. M., Tibre R.-A. & Han, T. (2024) *Supplementary Material of the paper C.-A. Bojan-Dragos, R.-E. Precup, E. M. Petriu, R.-A. Tibre and T. Han, Sliding Mode and Super-twisting Sliding Mode Control Structures for Vertical Three-tank Systems, Studies in Informatics and Control, 2024.* http://www.aut.upt.ro/~rprecup/Supplementary_material_SIC_2024.pdf

Bojan-Dragos, C.-A., Precup, R.-E., Preitl, S., Roman, R. C., Hedrea, E.-L. & Szedlak-Stinean, A.-I. (2021) GWO-based Optimal Tuning of Type-1 and Type-2 Fuzzy Controllers for Electromagnetic Actuated Clutch Systems, *IFAC-PapersOnLine*. 54(4), 189-194. doi: 10.1016/j.ifacol.2021.10.032.

Bouzouita, B., Bouani, F., Wertz, W. & Ksouri, M. (2008) Implementation of SISO Robust Predictive Control to a Three Tanks System. In: *Proceedings of 2008 IEEE International Conference on Control Applications, 3-5 September 2008, San Antonio, TX, USA*. IEEE. pp. 323-328.

Chakravarthi, M. K., Pannem, V. K. & Venkatesan, N. (2014) Real Time Implementation of Gain Scheduled Controller Design for Higher Order Nonlinear System Using LabVIEW. *International Journal of Engineering & Technology*. 6(5), 2031-2038.

Chen, B., Peng, W. & Song, J. (2023) A Frequent Construction Mining Scheme Based on Syntax Tree. *Romanian Journal of Information Science and Technology*. 26(1), pp. 3-20. doi: 10.59277/ROMJIST.2023.1.01.

Ćojbašić, Ž. M., Nikolić, V. D., Ćirić, I. T. & Ćojbašić, L. R. (2011) Computationally Intelligent Modeling and Control of Fluidized Bed Combustion Process. *Thermal Science*. 15(2), pp. 321-338. doi: 10.2298/TSCI101205031C.

Delavari, H., Ghaderi, R., Ranjbar, A. & Momani, S. (2010) Fuzzy Fractional Order Sliding Mode Controller for Nonlinear Systems. *Communications in Nonlinear Science and Numerical Simulation*. 15(4), 963-978. doi: 10.1016/j.cnsns.2009.05.025.

Dinesh Kumar, D. & Meenakshipriya, B. (2012) Design and Implementation of Nonlinear System Using Gain Scheduled PI controller. *Procedia Engineering*. 38, 3105-3112. doi: 10.1016/j.proeng.2012.06.361.

Emebu, S., Kubalčík, M., Backi, C. J. & Janáčová, D. (2023) A Comparative Study of Linear and Nonlinear Optimal Control of a Three-Tank System. *ISA Transactions*. 132, 419-427. doi: 10.1016/j.isatra.2022.06.002.

Filip, F. G. (2021) Automation and Computers and Their Contribution to Human Well-being and Resilience. *Studies in Informatics and Control*. 30(4), 5-18. doi: 10.24846/v30i4y202101.

Haber-Haber, R., Haber, R., Schmittdiel, M. & del Toro, R. M. (2007) A Classic Solution for the Control of a High-performance Drilling Process. *International Journal of Machine Tools and Manufacture*. 47(15), 2290-2297. doi: 10.1016/j.ijmachtools.2007.06.007.

Hedrea, E.-L., Precup, R.-E., Bojan-Dragos, C.-A., Hedrea, C., Ples, D. & Popovici, D. (2019) Cascade Control Solutions for Level Control of Vertical Three Tank Systems. In: *Proceedings of 2019 IEEE 13th International Symposium on Applied Computational Intelligence and Informatics (SACI), 29-31 May 2019, Timisoara, Romania*. IEEE. pp. 1-6.

Hirpara, R. H. (2022) State Estimation of Permanent Magnet Synchronous Motor Dynamics Using Higher-order Continuous-Discrete Filtering Equations. *Romanian Journal of Information Science and Technology*. 25(3-4), 303-321.

Hosokawa, A., Mitsuhashi, Y., Satoh, K. & Yang, Z.-J. (2023) Output feedback full-order sliding mode control for a three-tank system. *ISA Transactions*. 133, 184-192, 2023. doi: 10.1016/j.isatra.2022.06.038.

Inteco. (2007) *Multitank System, User's Manual*. Krakow, Inteco Ltd.

Johanyak, Z. C. (2017) A Modified Particle Swarm Optimization Algorithm for the Optimization of a Fuzzy Classification Subsystem in a Series Hybrid Electric Vehicle. [*Technical Gazette*]. 24(2), 295-301. doi: 10.17559/TV-20151021202802.

ICI Bucharest © Copyright 2012-2024. All rights reserved

Khalid, K. M. & Spurgeon, S. K. (2006) Robust MIMO Water Level Control in Interconnected Twin-tanks Using Second Order Sliding Mode Control. *Control Engineering Practice*. 14(4), 375-386. doi: 10.1016/j.conengprac.2005.02.001.

Klancar, G. & Blazic, S. (2019) Optimal Constant acceleration Motion Primitives. *IEEE Transactions on Vehicular Technology*. 68(9), 8502-8511. doi: 10.1109/TVT.2019.2927124.

Lascu, C., Boldea, I. & Blaabjerg, F. (2013) Super-twisting Sliding Mode Control of Torque and Flux in Permanent Magnet Synchronous Machine Drives. In: *Proceedings of 39th Annual Conference of the IEEE Industrial Electronics Society, 10-13 November 2013, Vienna, Austria*. IEEE. pp. 3171-3176.

Levant, A. (2003) Higher-order Sliding Modes, Differentiation and Output Feedback Control. *International Journal of Control*. 76(9-10), 924-941. doi: 10.1080/0020717031000099029.

Levant, A. (2005) Quasi-continuous Higher-order Sliding-mode Controllers. *IEEE Transactions on Automatic Control*. 50(11), 1812-1816. doi: 10.1109/TAC.2005.858646.

Levant, A. (2007) Principles of 2-sliding Mode Design. *Automatica*. 43(4), 576-586. doi: 10.1016/j.automatica.2006.10.008.

Meng, X., Yu, H., Zhang, J., Xu, T., Wu, H. & Yan, K. (2022) Disturbance Observer-based Feedback Linearization Control for a Quadruple-Tank Liquid Level System. *ISA Transactions*. 122, 146-162. doi: 10.1016/j.isatra.2021.04.021.

Milić, P., Marinković, D., Klinge, S. & Ćojbašić, Ž. (2023) Reissner-Mindlin Based Isogeometric Finite Element Formulation for Piezoelectric Active Laminated Shells. *Tehnički Vjesnik*. 30(2), 416-425. doi: 10.17559/TV-20230128000280.

Mirzaee, A. & Salahshoor, K. (2012) Fault Diagnosis and Accommodation of Nonlinear Systems Based on Multiple-model Adaptive Unscented Kalman Filter and Switched MPC and H-Infinity Loop-shaping Controller. *Journal of Process Control*. 22(3), 626-634. doi: 10.1016/j.jprocont.2012.01.002.

Orani, N., Pisano, A. & Usai, E. (2009) Fault Detection and Reconstruction for a Three-tank System via High-order Sliding-Mode Observer. In: *Proceedings of 2009 IEEE International Conference on Control Technology and Applications, 8-10 July 2009, Saint Petersburg, Russia*. IEEE. pp. 1714-1719.

Orani, N., Pisano, A. & Usai, E. (2010) Fault Diagnosis for the Vertical Three-tank System via High-order Sliding-Mode Observation. *Journal of the Franklin Institute*. 347(6), 923-939. doi: 10.1016/j.jfranklin.2009.11.010.

Precup, R.-E., David, R.-C., Petriu, E. M., Szedlak-Stinean, A.-I. & Bojan-Dragos, C.-A. (2016) Grey Wolf Optimizer-based Approach to the Tuning of PI-fuzzy controllers with a Reduced Process Parametric Sensitivity. *IFAC-PapersOnLine*. 495, 55-60. doi: 10.1016/j.ifacol.2016.07.089.

Precup, R.-E., Haidegger, T., Preitl, S., Benyo, Z., Paul, A. S. & Kovacs, L. (2012) Fuzzy Control Solution for Telesurgical Applications. *Applied and Computational Mathematics*. 11(3), 378-397.

Precup, R.-E., Tomescu, M. L., Preitl, S., Petriu, E. M., Fodor, J. & Pozna, C. (2013) Stability Analysis and Design of a Class of MIMO Fuzzy Control Systems. *Journal of Intelligent & Fuzzy Systems*. 25(1), 145-155. doi: 10.3233/IFS-2012-0621.

Precup, R.-E., Voisan, E.-I., Petriu, E. M., Tomescu, M. L., David, R. C., Szedlak-Stinean, A. I. & Roman, R.-C. (2020) Grey Wolf Optimizer-based Approaches to Path Planning and Fuzzy Logic-based Tracking Control for Mobile Robots. *International Journal of Computers Communications & Control*. 15(3), 1-17. doi: 10.15837/ijccc.2020.3.3844.

Preitl, S. & Precup, R.-E. (1996) On the Algorithmic Design of a Class of Control Systems Based on Providing the Symmetry of Open-loop Bode Plots. *Scientific Bulletin of UPT, Transactions on Automatic Control and Computer Science*. 41(2), 47-55.

Radiša, R., Dučić, N., Manasijević, S., Marković, N. & Ćojbašić, Ž. (2017) Casting Improvement Based on Metaheuristic Optimization and Numerical Simulation. *Facta Universitatis, Series: Mechanical Engineering*. 15(3), 397-411. doi: 10.22190/FUME170505022R.

Romero, S. V., Osaba, E., Villar-Rodriguez, E., Oregi, I. & Ban, Y. (2023) Hybrid Approach for Solving Real-world Bin Packing Problem Instances Using Quantum Annealers. *Scientific Reports*. 13(1), 11777. doi: 10.1038/s41598-023-39013-9.

Shah, D. H. & Patel, D. M. (2019) Design of Sliding Mode Control for Quadruple-tank MIMO Process with Time Delay Compensation. *Journal of Process Control*. 76, 46-61. doi: 10.1016/j.jprocont.2019.01.006.

Vascak, J., Hvizdo, J. & Puheim, M. (2016) Agent-based Cloud Computing Systems for Traffic Management. In: *Proceedings of 2016 International Conference on Intelligent Networking and Collaborative Systems, 7-9 September 2016, Ostrava, Czech Republic*. IEEE. pp. 73-79.

Vrcan, Ž., Troha, S., Marković, K. & Marinković, D. (2024) Analysis of Complex Planetary Gearboxes. *Spectrum of Mechanical Engineering and Operational Research*. 1(1), 227-249. doi: 10.31181/smeor11202420.